AD-A160 393 PNS (PARABOLIZED NAVIER-STOKES) COMPUTATIONS FOR SPINNING AND FIN-STABILI..(U) ARMY BALLISTIC RESEARCH LAB ABERDEEN PROVING GROUND MD P WEINACHT ET AL. 1/1

UNCLASSIFIED SEP 85 BRL-MR-3464 F/G 19/4 NL

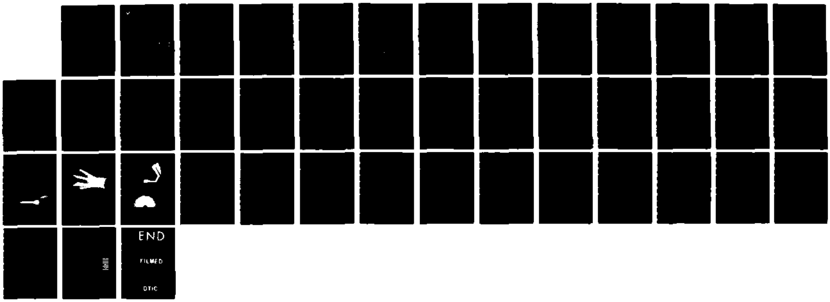

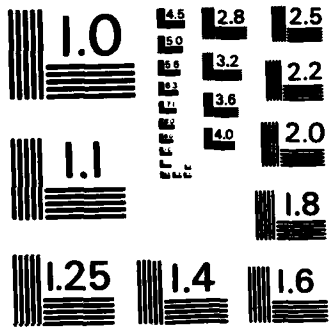

MICROCOPY RESOLUTION TEST CHART
NATIONAL BUREAU OF STANDARDS-1963-A

(12)

AD

US ARMY MATERIEL COMMAND

MEMORANDUM REPORT BRL-MR-3464

AD-A160 393

PNS COMPUTATIONS FOR SPINNING AND FIN-STABILIZED PROJECTILES AT SUPERSONIC VELOCITIES

Paul Weinacht
Bernard J. Guidos
Lyle D. Kayser
Walter B. Sturek

September 1985

US ARMY BALLISTIC RESEARCH LABORATORY
ABERDEEN PROVING GROUND, MARYLAND

85 10 15 074

UNCLASSIFIED

SECURITY CLASSIFICATION OF THIS PAGE (When Data Entered)

REPORT DOCUMENTATION PAGE

READ INSTRUCTIONS BEFORE COMPLETING FORM

1. REPORT NUMBER Memorandum Report BRL-MR-3464	2. GOVT ACCESSION NO. AD-A160 393	3. RECIPIENT'S CATALOG NUMBER
4. TITLE (and Subtitle) PNS COMPUTATIONS FOR SPINNING AND FIN-STABILIZED PROJECTILES AT SUPERSONIC VELOCITIES		5. TYPE OF REPORT & PERIOD COVERED 6. PERFORMING ORG. REPORT NUMBER
7. AUTHOR(s) P. Weinacht, B. J. Guidos, L. D. Kayser and W. B. Sturek		8. CONTRACT OR GRANT NUMBER(s)
9. PERFORMING ORGANIZATION NAME AND ADDRESS U.S. Army Ballistic Research Laboratory ATTN: AMXBR-LFD Aberdeen Proving Ground, Maryland 21005-5066		10. PROGRAM ELEMENT, PROJECT, TASK AREA & WORK UNIT NUMBERS RDT&E 1L162618AH80
11. CONTROLLING OFFICE NAME AND ADDRESS US Army Ballistic Research Laboratory (AMXBR-OD-ST) Aberdeen Proving Ground, Maryland 21005-5066		12. REPORT DATE September 1985 13. NUMBER OF PAGES 39
14. MONITORING AGENCY NAME & ADDRESS(if different from Controlling Office)		15. SECURITY CLASS. (of this report) Unclassified 15a. DECLASSIFICATION/DOWNGRADING SCHEDULE

16. DISTRIBUTION STATEMENT (of this Report)

Approved for public release, distribution unlimited

17. DISTRIBUTION STATEMENT (of the abstract entered in Block 20, if different from Report)

18. SUPPLEMENTARY NOTES

19. KEY WORDS (Continue on reverse side if necessary and identify by block number)

Computational Fluid Dynamics; Finned Projectiles; Three-Dimensional Flow; Supersonic Viscous Flow; Parabolized Navier-Stokes; Spinning Projectiles.

20. ABSTRACT (Continue on reverse side if necessary and identify by block number)

The Parabolized Navier-Stokes (PNS) computational technique has been applied to calculate the three-dimensional viscous flow about a standard spinning projectile and a long L/D finned projectile. The results for the spinning projectile are compared with past PNS computations and wind tunnel pressure and force measurements in order to benchmark the updated version of the code. Excellent agreement is found and the improvements to the code are shown to provide greater computational efficiency. Results are then presented for the

DD FORM 1473, 1 JAN 73 EDITION OF 1 NOV 65 IS OBSOLETE

UNCLASSIFIED

SECURITY CLASSIFICATION OF THIS PAGE (When Data Entered)

20. ABSTRACT (Continued)

finned projectile configuration and comparison made with predictions from an inviscid code and values from a data base compiled from range firings.

Keywords: →

TABLE OF CONTENTS

LIST OF ILLUSTRATIONS

LIST OF TABLES

I. INTRODUCTION

Application of the Parabolized Navier-Stokes (PNS) technique to predict the three-dimensional viscous flow about slender bodies of revolution at supersonic speeds and small angles of attack has been performed in the past with a considerable degree of success.[1-3] Of particular significance to the US Army is the capability that this technique provides in the prediction of the Magnus force and moment for spinning shell.[1-2] In light of this success, the PNS technique has been extended to examine the aerodynamics of more complexly configured projectiles, such as finned bodies. This paper documents the application of the PNS technique to a finned projectile configuration, resembling a long L/D kinetic energy (KE) penetrator projectile, and to a standard spinning projectile.

The PNS technique is a space-marching procedure in which the solution is marched spacially down the body in the main direction of the flow. It can be applied to problems for which the flow is supersonic and does not contain imbedded regions of subsonic flow or regions where the flow separates in the marching direction. For this class of problems, the PNS technique can be computationally more efficient, requiring less computer time and storage, compared with three-dimensional Navier-Stokes time-dependent procedures.

As the technique has evolved from the shock capturing code applied by Sturek, et al.,[1-3] significant improvements have been made, enabling this technique to be applied to the finned projectile configuration of interest. These improvements, several of which have been made by Rai, Chaussee, et al.,[4,5] include implementation of implicit shock-fitting boundary conditions, implicit smoothing terms, a force package cast in generalized geometry form, and an elliptic grid generator which produces the grid over the finned portion of the projectile. The implementation of the implicit shock-fitting boundary

---

1. *W. B. Sturek, D. C. Mylin, and C. C. Bush, "Computational Parametric Study of the Aerodynamics of Spinning Bodies at Supersonic Speeds," U.S. Army Ballistic Research Laboratory, Aberdeen Proving Ground, Maryland, ARBRL-TR-02358, August 1981. (AD A106074)*

2. *W. B. Sturek, and L. B. Schiff, "Computations of the Magnus Effect for Slender Bodies in Supersonic Flow," U.S. Army Ballistic Research Laboratory, Aberdeen Proving Ground, Maryland, ARBRL-TR-02384, December 1981. (AD A110016)*

3. *L. B. Schiff, and W. B. Sturek, "Numerical Simulation of Steady Supersonic Flow Over an Ogive Cylinder Boattail Body," U.S. Army Ballistic Research Laboratory, Aberdeen Proving Ground, Maryland, ARBRL-TR-02363, September 1981. (AD A106060)*

4. *M. M. Rai, and D. S. Chaussee, "New Implicit Boundary Procedures: Theory and Applications," AIAA Paper No. 83-0123, 21st Aerospace Sciences Meeting, January 1983.*

5. *M. M. Rai, D. S. Chaussee, Y. M. Rizk, "Calculation of Viscous Supersonic Flows over Finned Bodies," AIAA Paper No. 83-1667, Danvers, MA, July 1983.*

conditions has contributed to faster rates of convergence for the conical starting procedure and allowed larger stepsizes to be taken in the marching direction without loss of accuracy or stability. Use of implicit smoothing has been required in order to obtain solutions over the finned portion of the body.

In light of these improvements, application of the technique is first made to a standard shell configuration (SOCBT) to establish a benchmark for the code, which is henceforth denoted as FINPNS. Comparison with previous PNS calculations and wind tunnel data is made and the new capabilities evaluated. Results for the finned projectile configuration are then shown and compared with the NSWC Euler code (SWINT) and experimental data base values.

II. COMPUTATIONAL TECHNIQUE

Calculation of the flow field over the body is accomplished using the parabolized Navier-Stokes technique. The PNS technique allows the solution to be spacially marched along the body in the main flow direction due to the parabolic nature of the governing equations. An initial plane of data is required to begin the space marching procedure and may be obtained either from an auxiliary calculation or from a conical starting procedure, as has been done for the results presented here. Both the space marching and conical starting procedures are outlined below.

A. Space Marching Procedure

The thin-layer Parabolized Navier-Stokes computational technique developed by Schiff and Steger[6] has been employed to calculate the flow downstream of the nose. The governing steady thin-layer equations in strong conservative form and generalized coordinates are written below.

$$\frac{\partial \hat{E}_s}{\partial \xi} + \frac{\partial \hat{F}}{\partial \eta} + \frac{\partial \hat{G}}{\partial \zeta} = \frac{1}{\hat{Re}} \frac{\partial \hat{S}}{\partial \zeta} \qquad (1)$$

where ξ, η, ζ are the generalized coordinate variables as displayed in Figure 1.

$\xi = \xi(x)$ is the longitudinal (marching) coordinate

$\eta = \eta(x,y,z)$ is the circumferential coordinate

$\zeta = \zeta(x,y,z)$ is the near normal coordinate

This vector equation represents the thin-layer approximation to the equations of mass, momentum, and energy conservation in the three coordinate directions. The invisid flux vectors $\hat{E}_s$, $\hat{F}$, and $\hat{G}$ and the matrix of viscous

6. *L. B. Schiff, and J. L. Steger, "Numerical Simulation of Steady Supersonic Viscous Flow," AIAA Paper No. 79-0130, 17th Aerospace Sciences Meeting, January 1979.*

terms, $\hat{S}$, are functions of the dependent variables represented by the vector, $q(\rho, \rho u, \rho v, \rho w, e)$, where ρ is the density, u, v, and w are the velocity components in the three spacial directions x, y, and z, and e is the total energy per unit volume.

The parabolized Navier-Stokes equations are solved using a conservative, approximately factored, implicit, finite-difference numerical algorithm as formulated by Beam and Warming.[7] Further details of the numerical method may be found in Reference 6. Fitting of the outer bow shock has been performed in these calculations, and details of the implicit boundary procedure as implemented by Rai and Chaussee may be found in Reference 4. A fully turbulent boundary layer has been simulated in each of the reported calculations using a two-layer eddy viscosity model.[8,9]

B. Conical Starting Solutions

The initial plane of data required to begin the marching procedure is obtained using the marching code by assuming conical flow at the tip of the projectile. By selecting a conical grid and initially setting the flow field variables to the free stream values, the solution is marched one step down the body. The solution is then scaled back to the original station according to the conical flow assumption and again marched a single step. This procedure is repeated until a converged solution is obtained. The convergence criterion for the conical starting solutions applied here was that the change in density between successive iterations was less than 10^{-5} times the free stream value for each of the points on the body. This converged solution is then used as the initial plane of data in the marching procedure.

It should be noted that for calculations involving spinning projectiles, the conical starting procedure introduces a small error since the circumferential velocity at the body surface changes with longitudinal position, violating the conical flow assumption. This error is small, however, and the correct circumferential velocity at the body surface is accounted for as the solution is marched downstream.

III. RESULTS

A. SOCBT Configuration

In order to evaluate the new capabilities of the code, results were obtained for a secant-ogive-cylinder-boattail (SOCBT) projectile configuration

---

7. *R. Beam, and R. F. Warming, "An Implicit Factored Scheme for the Compressible Navier-Stokes Equations,"* AIAA Journal, *Vol. 16, No. 4, 1978, pp. 85-129.*

8. *B. S. Baldwin, and H. Lomax, "Thin Layer Approximation and Algebraic Model for Separated Turbulent Flows," AIAA Paper No. 78-257, 16th Aerospace Sciences Meeting, January 1978.*

9. *D. Degani, and L. B. Schiff, "Computation of Supersonic Viscous Flows Around Pointed Bodies at Large Incidence," AIAA Paper No. 83-0034, 21st Aerospace Sciences Meeting, January 1983.*

for which a significant amount of wind tunnel and computational results exist. A schematic of this projectile configuration is shown in Figure 2.

The grid for the current FINPNS computations consisted of 45 exponentially stretched points in the radial direction from the body to the shock and an equal spacing of points circumferentially around the body at 10 degree intervals. The benchmark PNS calculations[2] for the SOCBT configuration utilized the same circumferential spacing but used 50 points in the radial direction, clustering half the points near the body with the other half equispaced to a distance slightly beyond the shock to enable an outer shock capturing technique to be applied.

Conical starting solutions for the SOCBT were generated at a distance 4% of the total body length from the nosetip. Stepsizes for the conical starting procedure were adjusted to be as large as possible while still yielding stable solutions and accurate results in the marching mode. As noted in Reference 4, one criterion in selecting the proper stepsize is to maintain the maximum Courant number in the flow field at or below 12. The maximum Courant number for the current calculations was not permitted to exceed 10. In some cases, stepsizes for the current calculations were 2 to 5 times larger than those used for the previous PNS solutions to which comparisons were made. (A primary concern for the previous calculations was avoidance of departure solutions due to too large stepsizes.) A significant decrease in the number of steps for convergence was observed compared with the previous calculations, resulting in a substantial reduction in the CPU time for the procedure and is attributable to the implementation of the implicit boundary conditions and smoothing terms.

Results have been obtained for Mach numbers 2, 3, and 4, at 2 degree angle of attack, with and without spin for flow conditions duplicating those of the experiments.[10,11] All SOCBT results were generated on a CDC 7600 computer with a speed of 2.1 CPU sec/step for the stepback procedure and 4.2 CPU sec/step for the marching procedure.

Longitudinal surface pressure distributions for the Mach 3 non-spin case along the windward and leeward sides are shown in Figure 3. The comparison is good between the FINPNS computation and experiment, most notably in the vicinity of the discontinuities in streamwise surface curvature. Figure 4 shows circumferential pressure distributions at four axial locations on the projectile compared to experiment. The trends at all four axial locations agree well, and at the fourth station (on the boattail) the maximum disagreement

---

10. *R. P. Reklis, and W. B. Sturek, "Surface Pressure Measurements on Slender Bodies at Angle of Attack at Supersonic Speeds," U.S. Army Ballistic Research Laboratory, Aberdeen Proving Ground, Maryland, ARBRL-MR-02876, November 1978. (AD A064097)*

11. *C. J. Nietubicz, and K. O. Opalka, "Supersonic Wind Tunnel Measurements of Static and Magnus Aerodynamic Coefficients for Projectile Shapes with Tangent and Secant Ogive Noses," U.S. Army Ballistic Research Laboratory, Aberdeen Proving Ground, Maryland, ARBRL-MR-02991, February 1980. (AD A083297)*

between computation and experiment is less than 2%. For this case, the marching stepsize was increased by 5% every 10th step, so that the stepsize varies from .01 cal. at the starting plane to .037 cal. at the end of the projectile.

The effect of marching stepsize on the static forces (sign conventions shown in Figure 5) for the Mach 3 spin case is shown in Figures 6, 7, and 8. The normal force, Magnus force, and axial force (without base drag) are virtually unchanged using constant stepsizes of .008 and .027 cal. A third case shown in these same figures used a stepsize of .027 cal. at the starting plane and increased by 5% every 10th step to .053 cal. at the base of the projectile. The previous PNS solutions for this case used stepsizes in the range from .008 to .01 cal. A considerable amount of computational time is saved due to the fewer number of steps required to march completely over the body.

The effect of smoothing on these same forces at Mach 3 is demonstrated in Figures 9, 10, and 11. Table 1 lists the values of smoothing used to march each solution. Definition of the smoothing parameters discussed here is made in Reference 12. Run #1 represents the (minimal) type of smoothing needed to solve for a body-alone configuration at low angle of attack. Run #6 represents the typically large amounts of smoothing needed for high angle of attack solutions or finned body configurations. It is noteworthy that the normal force is most affected by the excessive amounts of dissipation being forced into the solution. On the other hand, axial force and Magnus coefficients appear to be less affected by excessive smoothing. For Run #6, the apparent lack of sensitivity of axial force to the excessive amounts of smoothing is caused by an offsetting of the pressure and viscous components of drag. The pressure drag experienced an increase of 10% over Run #1, while the viscous drag decreased by 30%.

TABLE 1. MARCHING SOLUTIONS; COMPARISON OF SMOOTHING PARAMETERS SOCBT, $M = 3$, $\alpha = 2°$, PD/V = .19 (20K RPM)

Solution #	DX (cal)	SMU	SMUIM	EPSA	EPSB
1	.027	.005	0.0	0.0	0.0
2	.027	.010	0.0	0.0	0.0
3	.027	.100	.25	0.0	0.0
4	.027	.200	.50	0.0	0.0
5	.027	.200	.50	0.1	0.2
6	.027	1.000	2.00	0.1	0.5

Figures 12 and 13 compare the FINPNS (Solution #2) and PNS solutions to experimental measurements at Mach 3. These graphs show the development of the normal and Magnus force coefficients over the body and provide additional

12. *D. S. Chaussee, J. L. Patterson, P. Kutler, T. Pulliam, and J. L. Steger, "A Numerical Simulation of Hypersonic Viscous Flows Over Arbitrary Geometries at High Angle of Attack," AIAA Paper 81-0050, January 1981.*

validation of the results from FINPNS. In addition, Table 2 lists values of the components of Magnus force coefficient; i.e., C_{p_w}, wall pressure component; C_{τ_ϕ}, circumferential wall shear; and C_{τ_x}, longitudinal wall shear. For all cases, an adaptive grid technique such as that mentioned in Reference 2 was used to control the grid resolution at the wall.

TABLE 2. COMPARISON OF MAGNUS FORCE COMPONENTS SOCBT, M = 3, α = 2°, PD/V = .19 (20K RPM)

	C_{τ_x}	C_{τ_ϕ}	C_{p_w}	C_Y
FINPNS (#2)	$+.097 \times 10^{-5}$	$.213 \times 10^{-3}$	$-.285 \times 10^{-2}$	-.00264
PNS	$-.147 \times 10^{-5}$	$.180 \times 10^{-3}$	$-.278 \times 10^{-2}$	-.00259
EXPERIMENT (Ref. 10)				-.00270

Figure 14 compares axial force coefficients (without base drag) for PNS and FINPNS calculations. The discrepancy between the two solutions was found to be caused by the fact that the FINPNS force package makes use of a second order Taylor series expansion of the velocities at the wall to define velocity gradients for calculations of shear stresses, while the previous PNS calculations employed a first order approximation. The FINPNS code was re-run using a first order Taylor series expansion to define wall velocity gradients and results for the viscous component of axial force compared with the second order accurate FINPNS result and with the previous PNS result, as shown in Figure 15. Both of the first order predictions of axial viscous force compare well, and the difference between the first and second order prediction accounts for the discrepancy in the total axial force. Normal and Magnus forces, which are primarily pressure forces, were not strongly dependent on the order of the Taylor series expansion used for wall velocity gradients.

Figures 16, 17, and 18 show the pitching moment coefficient, the pitch-plane center of pressure, and Magnus moment coefficient as a function of Mach number as predicted by the FINPNS and PNS codes, compared with the experiment. Excellent agreement between the predictions of the two codes and experiment are seen for the pitch-plane center of pressure and the pitching moment coefficient. Good agreement is seen between the predicted and experimental values for the Magnus moment coefficient at the higher values of Mach number, though this agreement falls off somewhat as the Mach number decreases. These results further document the suitability of the technique for the prediction of the supersonic flow about spinning projectiles.

B. Finned Projectile Configuration

The finned body configuration for which calculations have been performed resembles closely the M735 Army projectile. The modeled finned body configuration is characterized by a conical nose section joined to a smooth cylindrical main body with six symmetrical swept fins attached to the aft section of the projectile. Figure 19 displays the basic dimensions of this configuration. The actual projectile differs from the modeled projectile in that the actual projectile has: (1) circumferential grooves over much of the cylindrical portion of the body to prevent the sabot from sliding off the body in the gun tube; (2) fins which have a non-symmetrical sectional geometry to induce roll; and (3) a slightly rounded nose. Modeling the projectile with a sharp nose and a symmetrical fin section are not the result of inherent limitations of the computational model, but rather a matter of convenience for these initial calculations. While modeling of the sabot grooves may be possible using surface blowing, wind tunnel results have shown that such grooves have almost no effect on the value of normal force and pitching moment. These grooves do, however, have a noticeable effect on drag, particularly at higher angles of attack.[13]

A shadowgraph of the actual projectile in flight at Mach 4.3 is shown in Figure 20 and displays some of the relevant features of the flow field; a bow shock wave emanating from the nose of the projectile, shocks at the leading edge of the fins, expansion waves at the cone-cylinder junction, and a boundary layer which increases along the body.

Results are presented here for Mach numbers of 3, 4, and 5, two degrees angle of attack, and turbulent flow conditions over the body. Atmospheric flight conditions were simulated by maintaining the body temperature at the free stream value of 294 K. Calculations were made with two of the fins oriented vertically, enabling a half plane of symmetry to be applied.

Generation of an initial plane of data using the conical starting procedure was performed at a position .36 calibers from the tip of the cone. Solutions were first converged for large values of explicit and implicit smoothing (see Table 3) and typically required 180 steps. Implicit smoothing was then removed, explicit smoothing reduced to a value of 0.015, and the solution reconverged with approximately an additional 450 steps. The starting solution for each Mach number was obtained using a step size of .0072 calibers, 19 circumferential points spaced equally in the half plane, and 45 constantly stretched points from the body surface to the shock. The spacing from the wall to the first point above the wall was adjusted so that the first point above the wall was in the laminar sublayer.

Using this initial plane of data, the solution was then marched down the cone and onto the cylinder to a position approximately one caliber in front of the fins. At this point the circumferential gridding was increased from 19 to 121 equally spaced points to improve the resolution for marching over the fins, and the solution marched to the beginning of the fins. Over the cone-cylinder portion of the body a step size of .0072 calibers, explicit smoothing of .015, and 45 points constantly stretched points from the body to the shock were used. Spacing from the wall to the first point above the wall was again maintained so that one point was in the laminar sublayer.

---

13. *F. Brandon, "private communications," U.S. Army Ballistic Research Laboratory, Aberdeen Proving Ground, Maryland.*

TABLE 3. SMOOTHING PARAMETERS FOR FINNED BODY CALCULATIONS

SMOOTHING PARAMETERS	CONE STARTS 1st Solution	CONE STARTS Final Solution	MARCHING MODE Cone-Cylinder	Fins M = 3	Fins M = 4	Fins M = 5
SMU	1.0	0.015	0.015	1.0	1.0	1.0
SMUIM	2.0	0.	0.	2.0	2.0	2.0
EPSA	1.0	0.	0.	0.1	1.-1.5	1.5
EPSB	1.0	0.	0.	0.5	1.-1.5	1.5

Once on the finned portion of the body, the grid was obtained through the use of an elliptic grid generator.[5] Points on the body surface were clustered near the leading edge of the fins, as shown in Figure 21. Figures 22a and b show a cross section of the grid on the finned portion of the body at an axial location of X/D = 13.2. Grid points are clustered near the body to resolve the boundary layer.

In marching the solution over the finned portion of the body, substantial difficulty was encountered in obtaining a solution, particularly at the axial locations near the beginning of the fins and at the axial location where the fins reach their maximum span. In addition to adding significant amounts of explicit and implicit smoothing (see Table 3), the distance from the wall to the first point above the wall had to be increased to a value ten times that used immediately in front of the fins in order to obtain a solution for a step size of .0072 calibers. Decreasing the step size by a factor of ten allowed the radial spacing at the wall to be reduced by a factor of three, but the resulting rise in computational time prohibited this approach. Solutions were obtained at Mach 4 and 5 for lower levels of smoothing, but oscillations of the pressure on the leading edge of the fins were evident. The higher levels of smoothing used damped these oscillations out without affecting the prediction of forces and moments significantly.

Figure 23, which displays the pressure along the body on the wind and lee sides and at a point in between, sheds some light on the reasons for the computational difficulties over the finned portion of the body. A sharp rise in pressure on the leading edge of the wind and lee fins is seen, followed by a sharp drop at the axial location where the fin reaches its maximum span.

Figures 24 and 25 show the development of the normal force coefficient and pitching moment coefficient (referenced to the center of gravity position, shown in Figure 19) over the body. The normal force coefficient shows a moderate contribution due to the conical nose and cylindrical portion of the body and larger contribution due to the finned portion of the body. The development of the pitching moment coefficient over the body demonstrates the stablizing influence of the fins, changing the pitching moment from a positive value to a large negative (stable) value at the aft end of the fins. In these figures comparison is made with results obtained with the NSWC inviscid code

(SWINT)[14] and LCWSL data[15] base values for the actual projectile configuration.

The SWINT code - SWINT is an acronym for Supersonic Wing INlet Tail - solves explicitly the Euler equations for supersonic flow over bodies with fins and/or wings, and for the external flow about bodies with inlets. The code makes use of the thin fin approximation, collapsing each fin along a single radial plane in the grid. Fin thickness can be accounted for in the code by application of the appropriate local analysis such as shock compression and Prandtl-Meyer expansion theories. The fin edges must be sharp and cannot extend beyond the bow shock. Additionally, the flowfield must remain supersonic throughout the entire computation.

Development of the normal force and pitching moment coefficients as predicted by the FINPNS and SWINT codes compare well. Good agreement between the total value of normal force and pitching moment for both procedures is seen compared with the LCWSL data.

Pressure distributions on the wind and lee sides of the $\phi = 120°$ fin at the 1/4 and 1/2 span positions are shown in Figure 26a and b compared with the SWINT code predictions. Differences in the predicted pressures at the leading edge of the fin are attributable to the thin-fin approximation applied for the SWINT calculations. The FINPNS code seems to predict a more even distribution of lift along the chord of the fin, while the SWINT predictions show slightly more lift being developed at the leading edge of the fin.

The variation of the predicted values of the slope of the normal force and pitching moment coefficients with Mach number is compared with the values predicted by the SWINT code and with LCWSL data in Figures 27-28. The FINPNS code is seen to overpredict the normal force and pitching moment coefficients compared with the LCWSL data, while the SWINT code gives generally better agreement.

The variation in the predicted center of pressure with Mach number is shown in Figure 29 and is also compared with values predicted by the SWINT code and with LCWSL data. Both codes predict similiar values of center of pressure and show good agreement with the LCWSL data.

IV. CONCLUSIONS

The application of the Parabolized Navier-Stokes Technique to a Secant-Ogive-Cylinder-Boattail (SOCBT) projectile has verified recent code improvements which allow the code to be utilized in an even more computationally efficient manner. This report has demonstrated that consistently accurate

---

14. *A. B. Wardlaw, Jr., F. P. Baltakis, J. M Soloman, and L. B. Hackerman, "An Inviscid Computational Method for Tactical Missile Configurations," NSWC TR 81-457.*

15. *Unpublished range lata, U.S. Army Ballistic Research Laboratory, Aberdeen Proving Ground, Maryland.*

results can be achieved for the SOCBT configuration at small angles of attack over a range of supersonic Mach numbers, establishing a satisfactory comparison against benchmark results.

Results of the FINPNS calculations for the finned projectile configuration have shown fair agreement with LCWSL data and Euler (SWINT) code predictions but further improvements are required before a satisfactory predictive capability can be considered to exist. Current levels of smoothing should probably be reduced and better resolution of the boundary layer on the fins is required. Implementation of a global iteration technique may help overcome some of these difficulties.

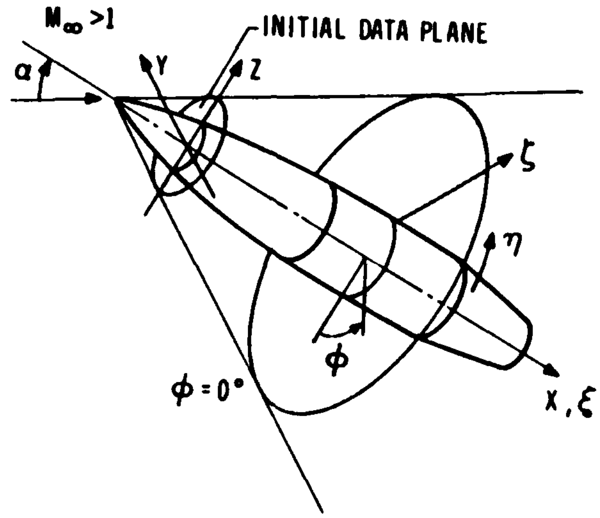

Figure 1. Grid Coordinates and Notations

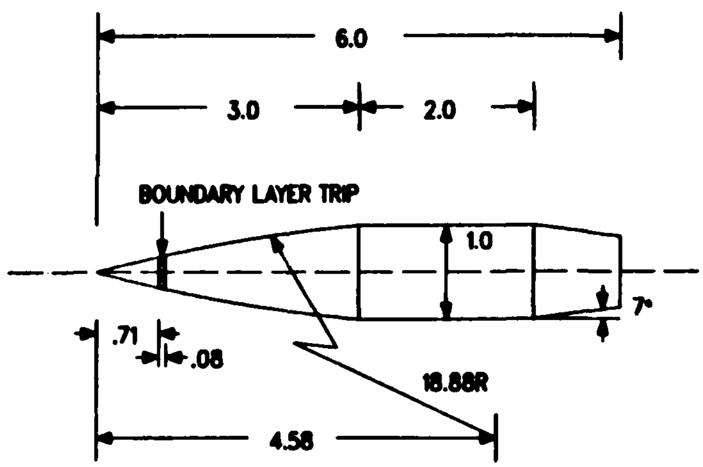

Figure 2. Secant Ogive-Cylinder-Boattail (SOCBT) Configuration

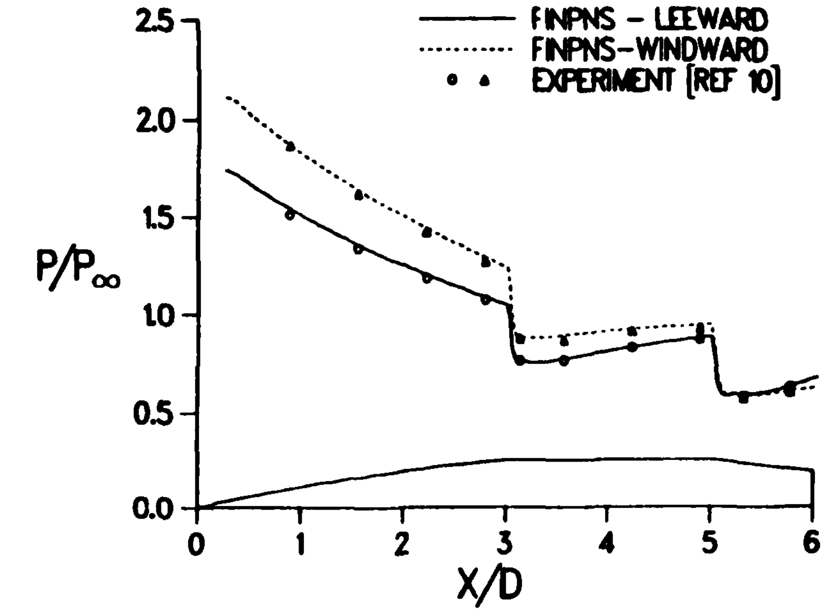

Figure 3. Longitudinal Surface Pressure Distribution on SOCBT Configuration; $M = 3$, $\alpha = 2°$, $PD/V = 0$, $Re_D = 1.2$ million

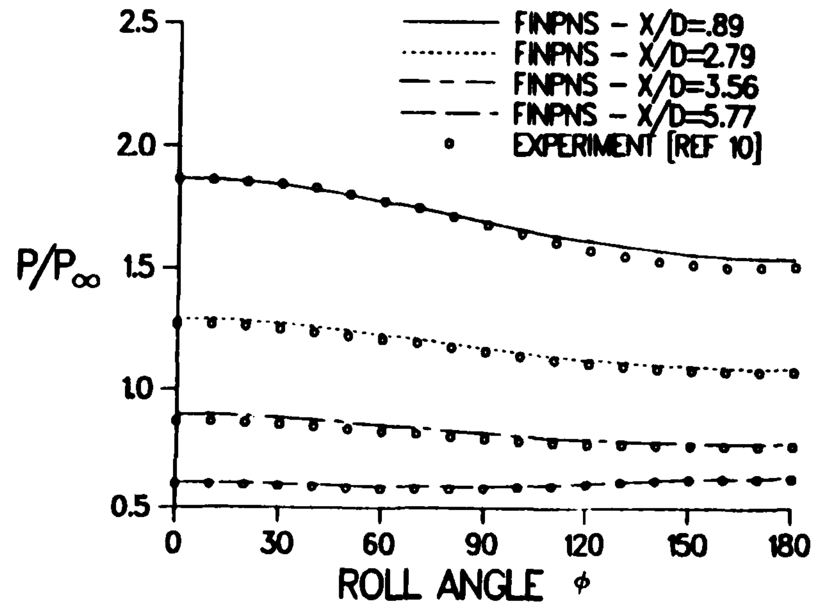

Figure 4. Circumferential Surface Pressure Distribution on SOCBT Configuration; $M = 3$, $\alpha = 2°$, $PD/V = 0$, $Re_D = 1.2$ million

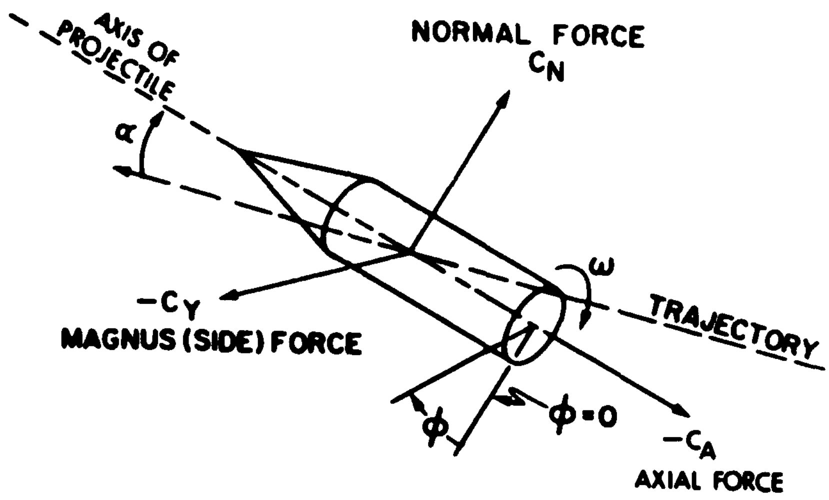

Figure 5. Sign Convention for Spin and Aerodynamic Force Coefficients

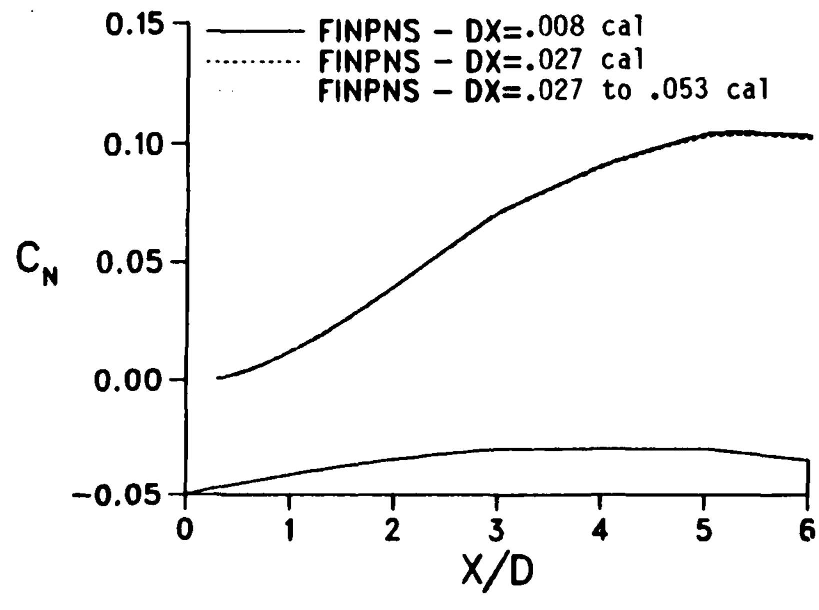

Figure 6. Total Normal Force Coefficient Developing over SOCBT Configuration; $M = 3$, $\alpha = 2°$, $PD/V = .19$, $Re_D = 1.2$ million

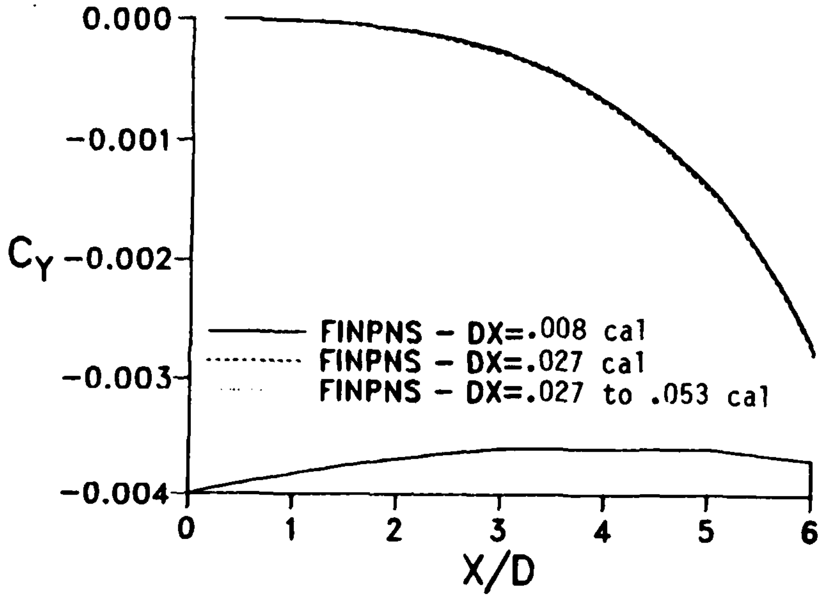

Figure 7. Total Magnus Force Coefficient Developing over SOCBT Configuration; $M = 3$, $\alpha = 2°$, $PD/V = .19$, $Re_D = 1.2$ million

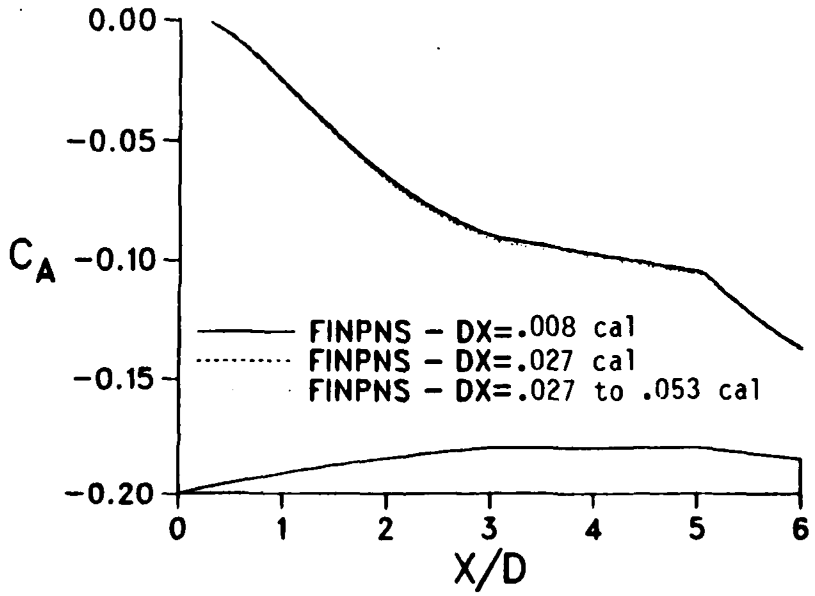

Figure 8. Total Axial Force Coefficient Developing over SOCBT Configuration; $M = 3$, $\alpha = 2°$, $PD/V = .19$, $Re_D = 1.2$ million

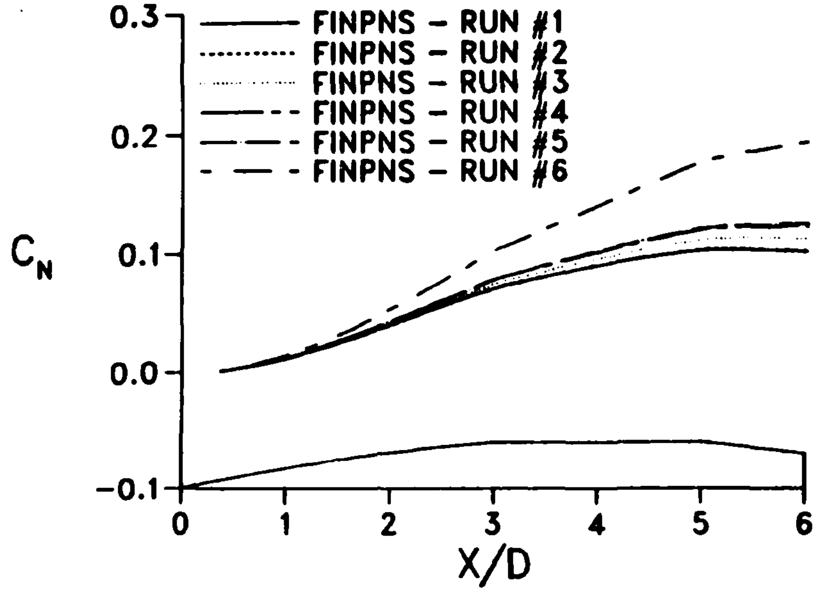

Figure 9. Total Normal Force Coefficient Developing over SOCBT Configuration; M = 3, α = 2°, PD/V = .19, Re_D = 1.2 million

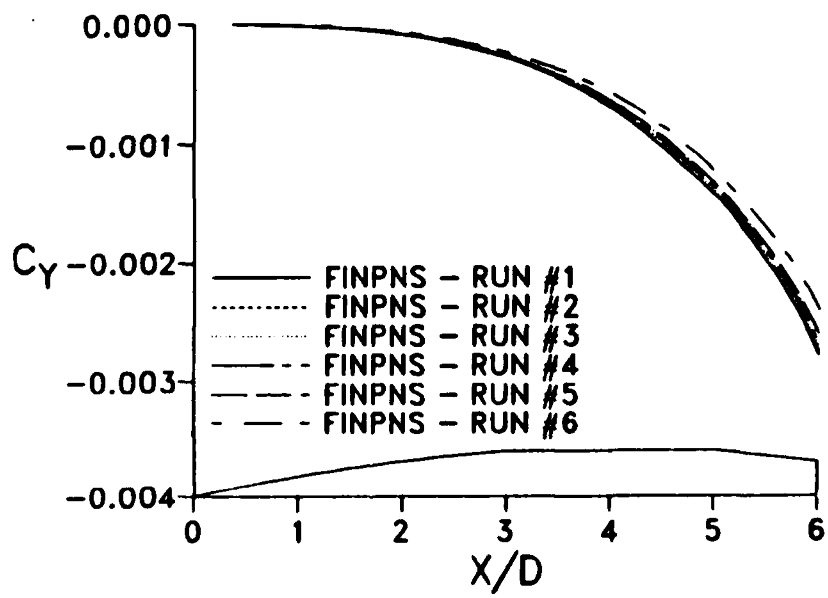

Figure 10. Total Magnus Force Coefficient Developing over SOCBT Configuration; M = 3, α = 2°, PD/V = .19, Re_D = 1.2 million

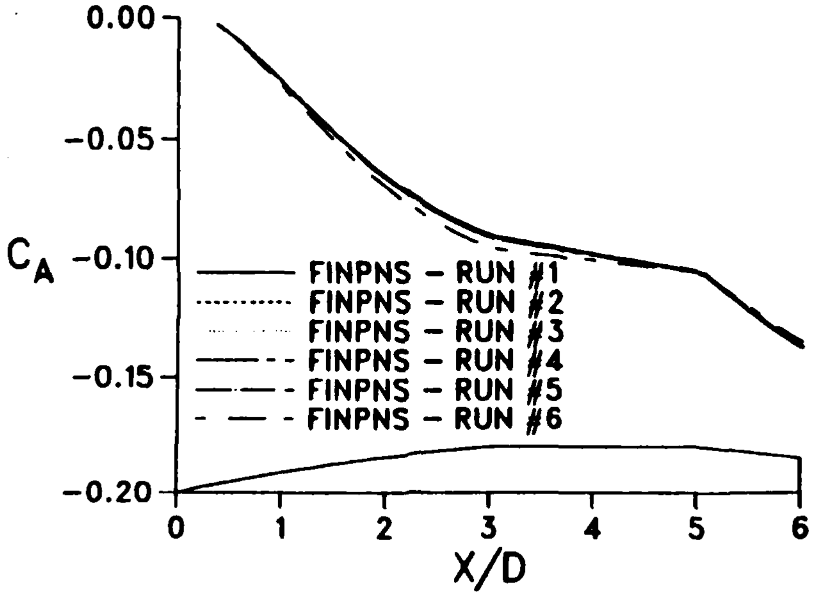

Figure 11. Total Axial Force Coefficient Developing over SOCBT Configuration; $M = 3$, $\alpha = 2°$, $PD/V = .19$, $Re_D = 1.2$ million

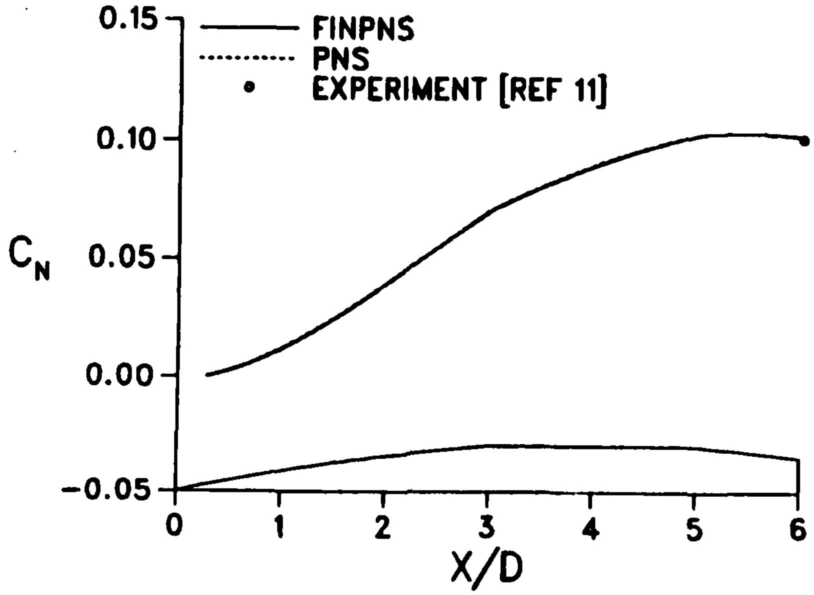

Figure 12. Total Normal Force Coefficient Developing over SOCBT Configuration; $M = 3$, $\alpha = 2°$, $PD/V = .19$, $Re_D = 1.2$ million

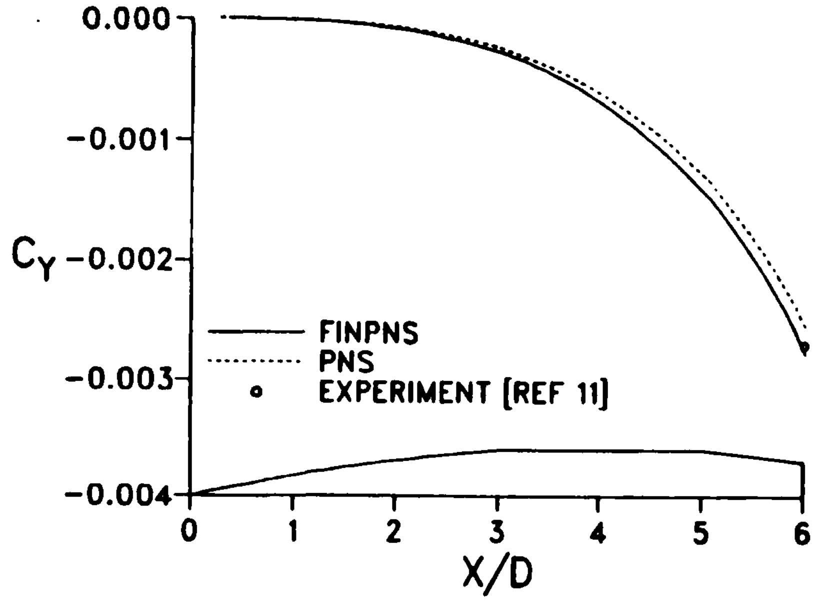

Figure 13. Total Magnus Force Coefficient Developing over SOCBT Configuration; M = 3, α = 2°, PD/V = .19, Re_D = 1.2 million

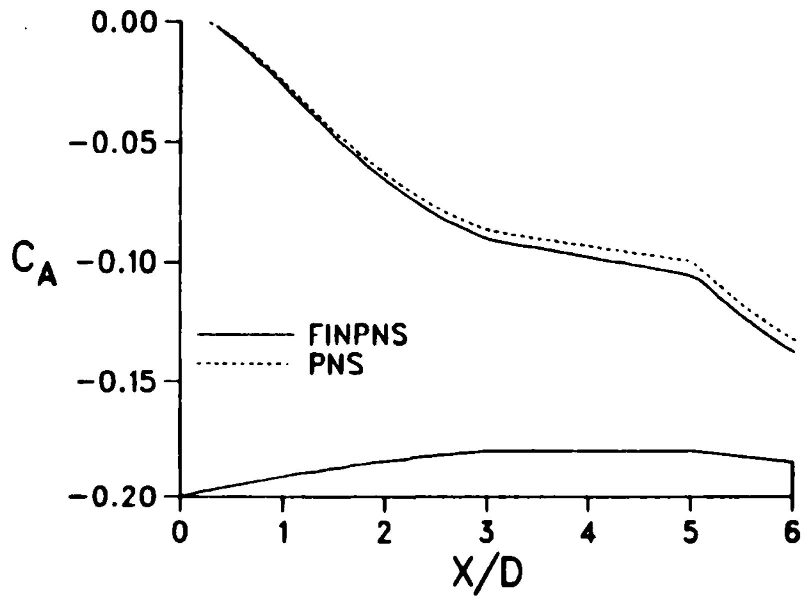

Figure 14. Total Axial Force Coefficient Developing over SOCBT Configuration; M = 3, α = 2°, PD/V = .19, Re_D = 1.2 million

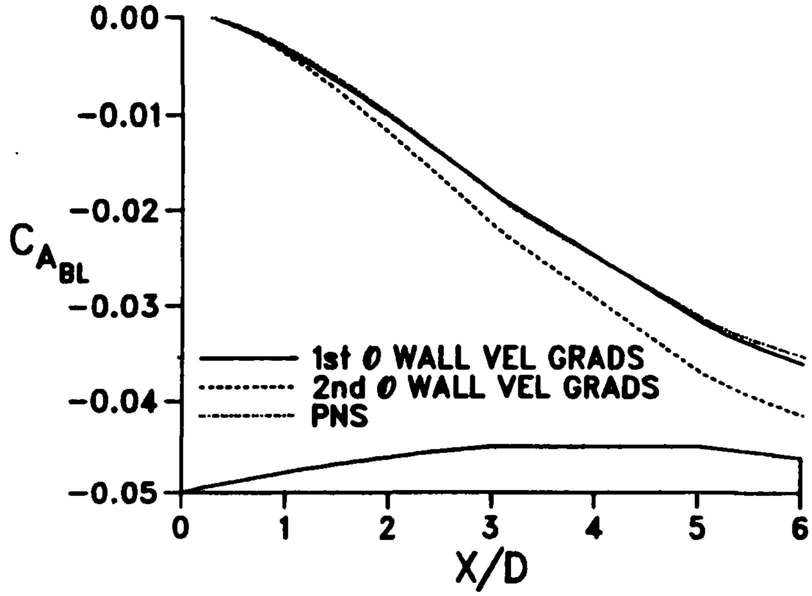

Figure 15. Viscous Component of Drag Coefficient Developing over SOCBT Configuration; M = 3, α = 2°, PD/V = .19, Re_D = 1.2 million

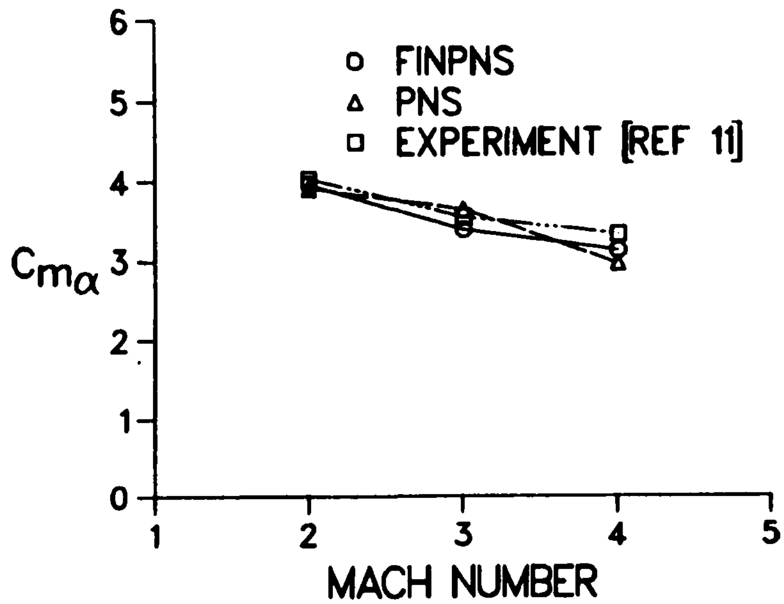

Figure 16. Slope of Pitching Moment Coefficient versus Mach Number for SOCBT Configuration

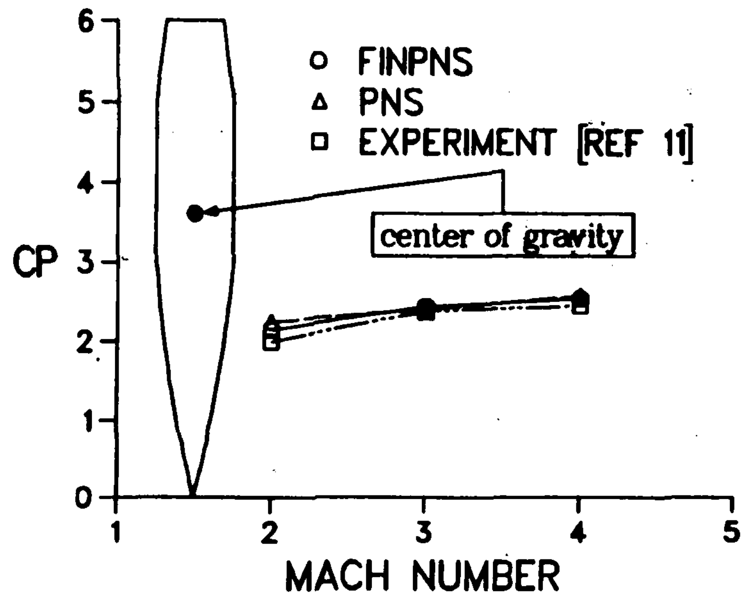

Figure 17. Normal Force Center of Pressure versus Mach Number for SOCBT Configuration

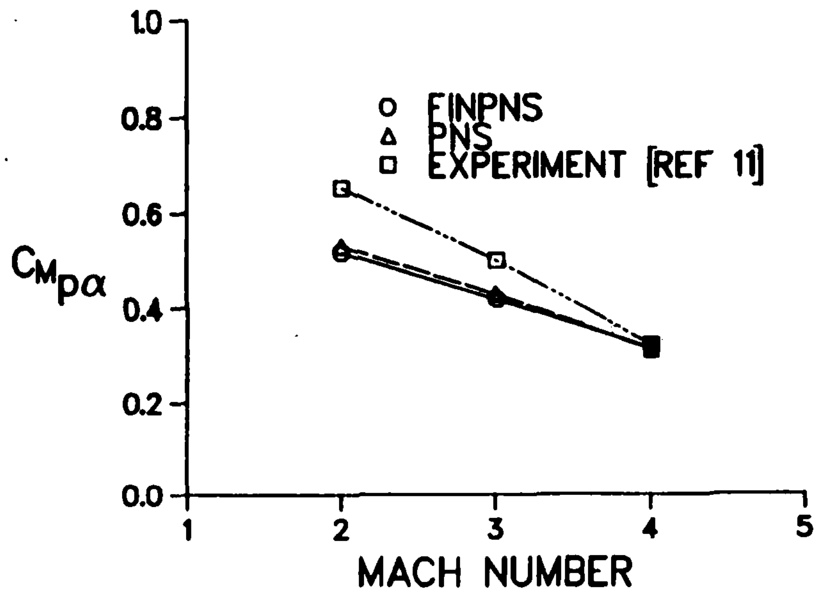

Figure 18. Slope of Magnus Moment Coefficient versus Mach Number for SOCBT Configuration

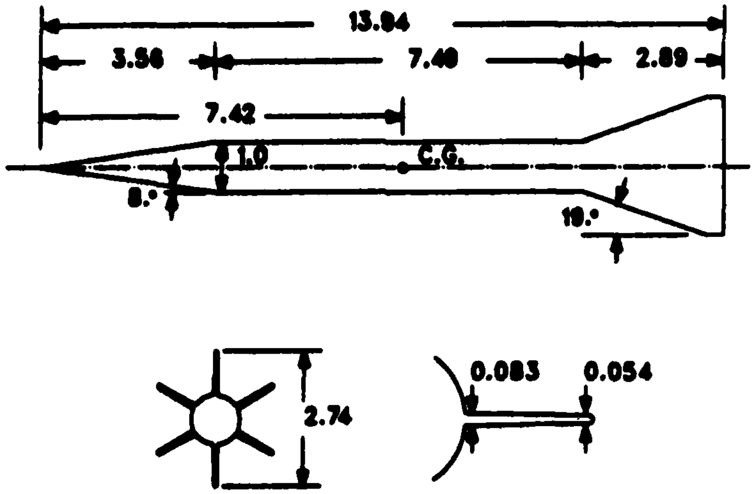

ALL DIMENSIONS IN CALIBERS (ONE CALIBER = 35.2 mm)

Figure 19. Finned Projectile Configuration

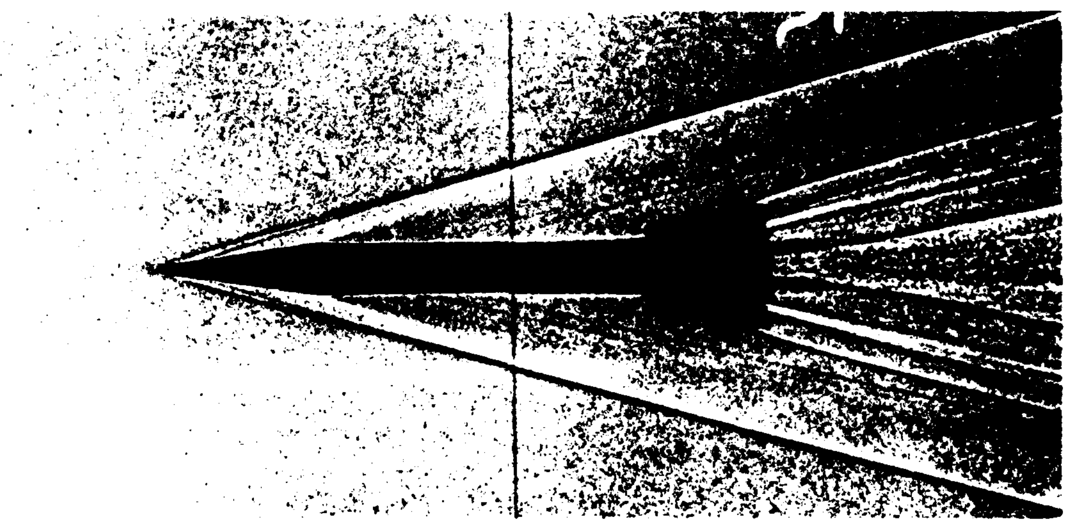

Figure 20. Shadowgraph of M735 Projectile in Flight

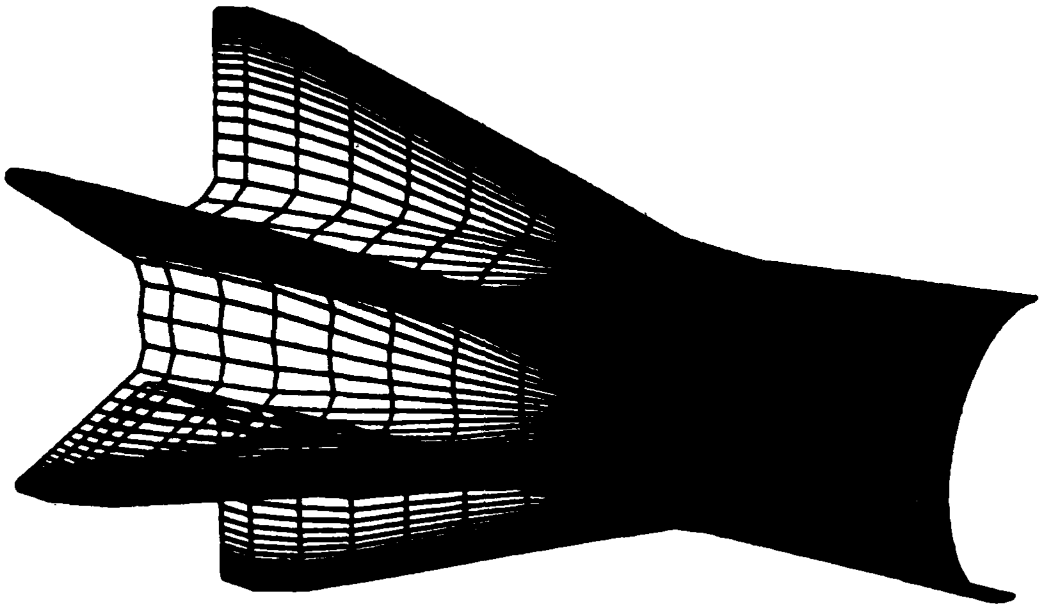

Figure 21. Grid on Body Surface on Finned Portion of Projectile

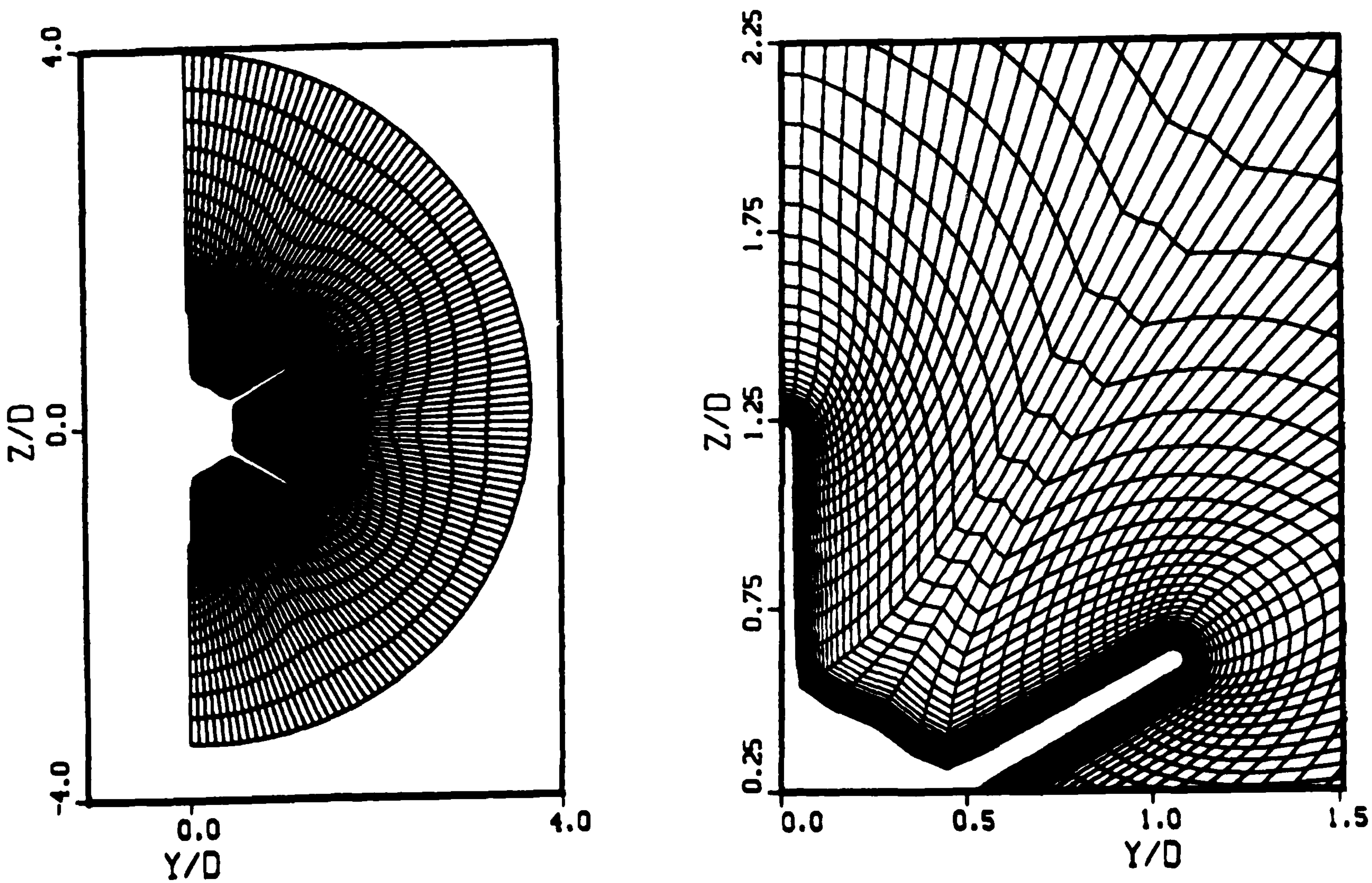

a. Half Plane Grid

b. Close-Up of Grid Near Body

Figure 22. Cross Section of Grid at X/D = 13.2

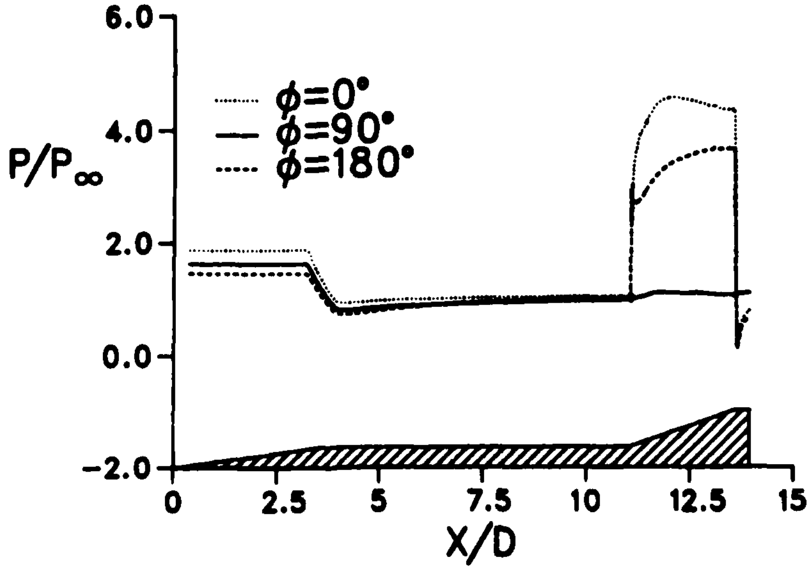

Figure 23. Axial Pressure Distribution at $\phi = 0°$, $\phi = 90°$, and $\phi = 180°$, $M = 4$, $\alpha = 2°$, $Re_D = 3.2$ million

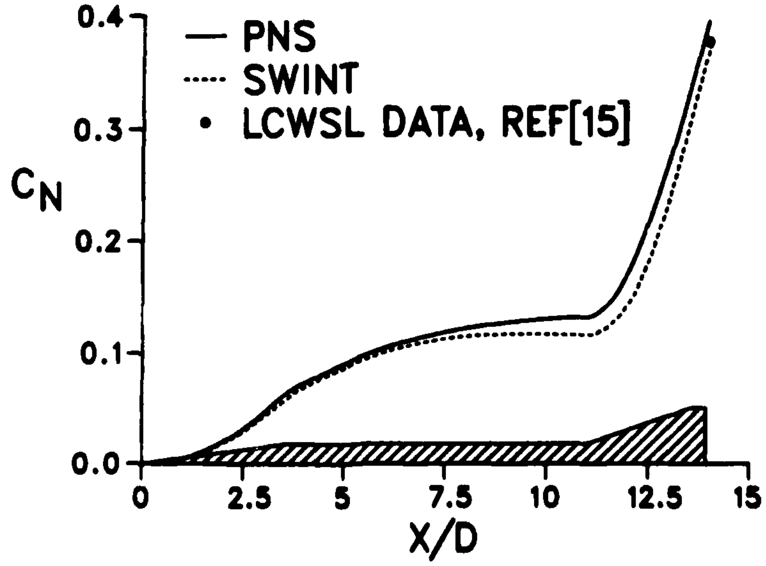

Figure 24. Development of Normal Force Coefficient along Body, $M = 4$, $\alpha = 2°$, $Re_D = 3.2$ million

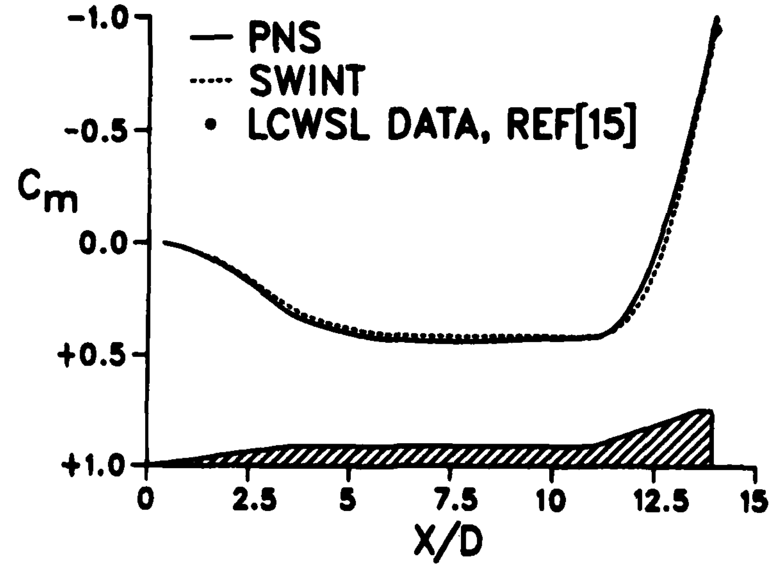

Figure 25. Development of Pitching Moment Coefficient along Body, M = 4, α = 2°, Re_D = 3.2 million

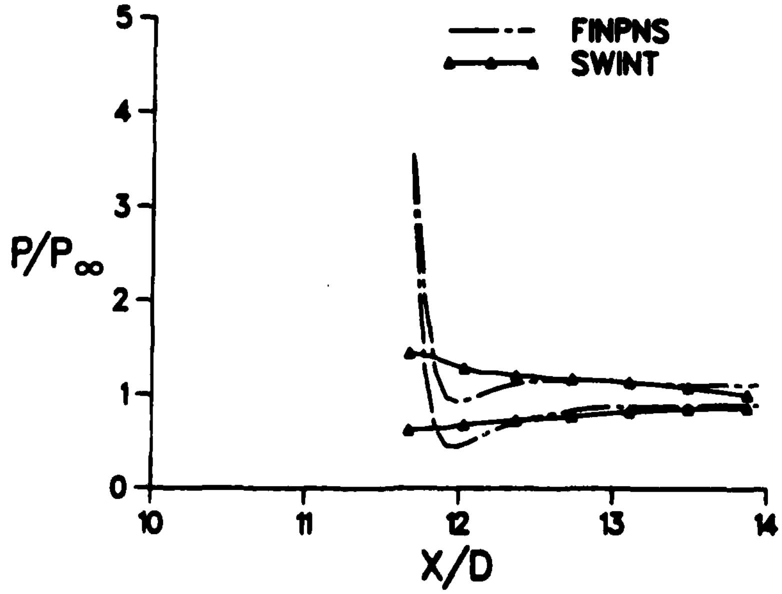

Figure 26a. Chordwise Pressure Distribution at 1/4 Span Position, ϕ = 120° Fin, M = 4, α = 2°, Re_D = 3.2 million

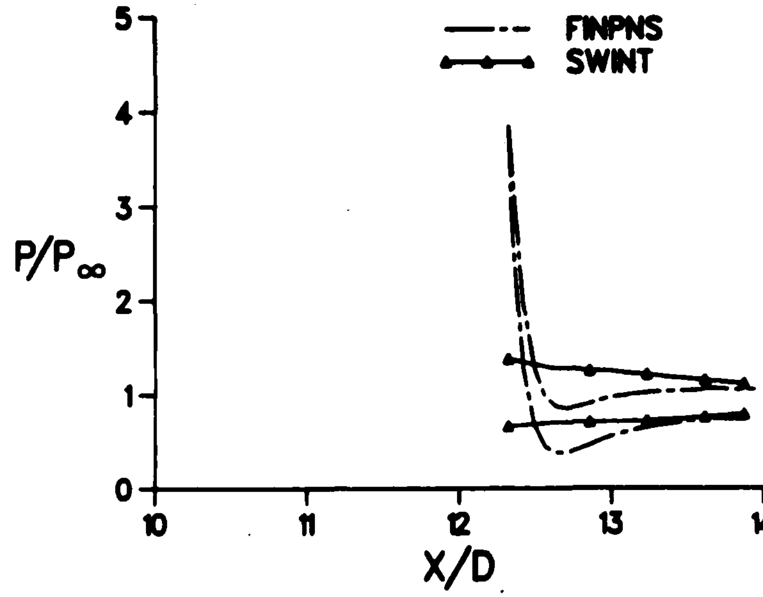

Figure 26b. Chordwise Pressure Distribution at 1/2 Span Position, ϕ = 120° Fin, M = 4, α = 2°, Re_D = 3.2 million

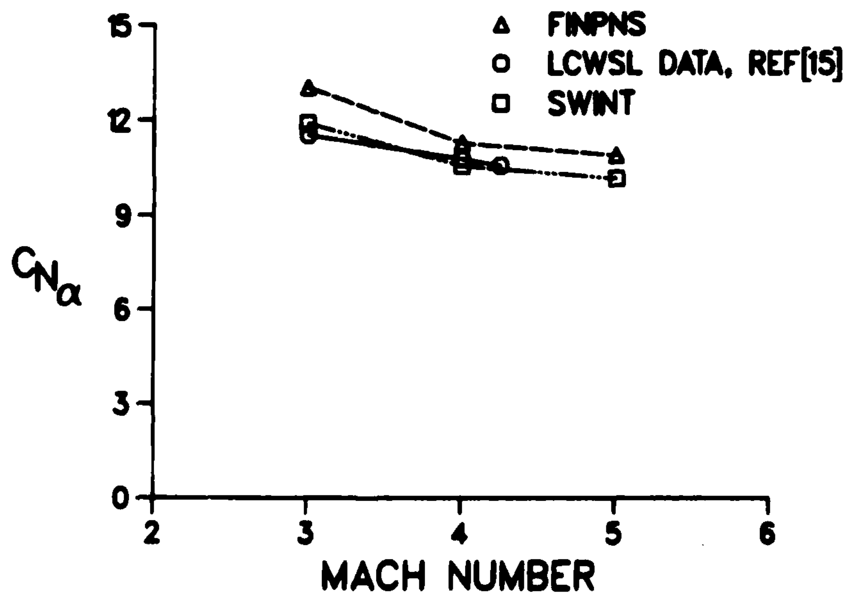

Figure 27. Zero-Degree Slope of the Normal Force Coefficient versus Mach Number

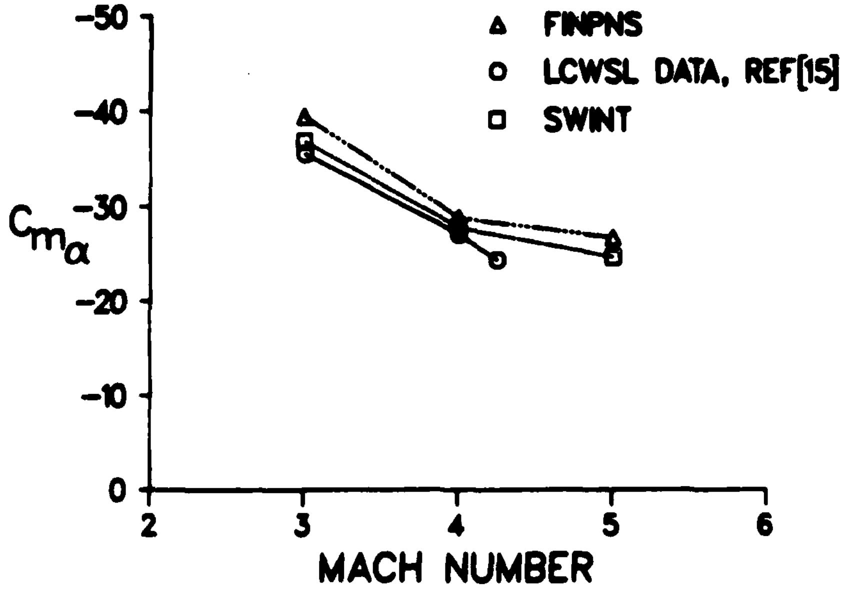

Figure 28. Zero-Degree Slope of the Pitching Moment Coefficient versus Mach Number

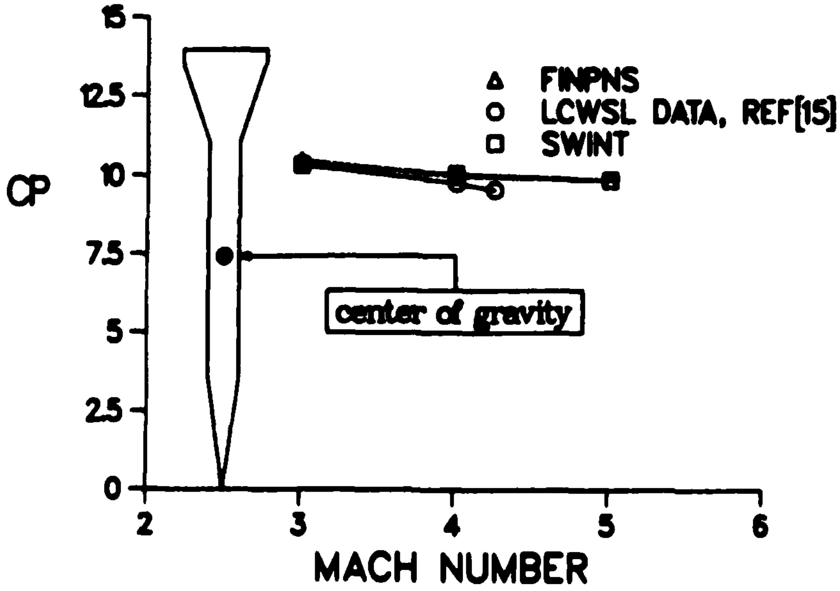

Figure 29. Normal Force Center of Pressure versus Mach Number

REFERENCES

1. W. B. Sturek, C. C. Mylin, and C. C. Bush, "Computational Parametric Study of the Aerodynamics of Spinning Bodies at Supersonic Speeds," U.S. Army Ballistic Research Laboratory, Aberdeen Proving Ground, Maryland, ARBRL-TR-02358, August 1981. (AD A106074)

2. W. B. Sturek, and L. B. Schiff, "Computations of the Magnus Effect for Slender Bodies in Supersonic Flow," U.S. Army Ballistic Research Laboratory, Aberdeen Proving Ground, Maryland, ARBRL-TR-02384, December 1981. (AD A110016)

3. L. B. Schiff, and W. B. Sturek, "Numerical Simulation of Steady Supersonic Flow Over an Ogive Cylinder Boattail Body," U.S. Army Ballistic Research Laboratory, Aberdeen Proving Ground, Maryland, ARBRL-TR-02363, September 1981. (AD A106060)

4. M. M. Rai, and D. S. Chaussee, "New Implicit Boundary Procedures: Theory and Applications," AIAA Paper No. 83-0123, 21st Aerospace Sciences Meeting, January 1983.

5. M. M. Rai, D. S. Chaussee, and Y. M. Rizk, "Calculation of Viscous Supersonic Flows over Finned Bodies," AIAA Paper No. 83-1667, Danvers, MA, July 1983.

6. L. B. Schiff, and J. L. Steger, "Numerical Simulation of Steady Supersonic Viscous Flow," AIAA Paper No. 79-0130, 17th Aerospace Sciences Meeting, January 1979.

7. R. Beam, and R. F. Warming, "An Implicit Factored Scheme for the Compressible Navier-Stokes Equations," AIAA Journal, Vol. 16, No. 4, 1978, pp. 85-129

8. B. S. Baldwin, and H. Lomax, "Thin Layer Approximation and Algebraic Model for Separated Turbulent Flows," AIAA Paper No. 78-257, 16th Aerospace Sciences Meeting, January, 1978.

9. D. Degani, and L. B. Schiff, "Computation of Supersonic Viscous Flows Around Pointed Bodies at Large Incidence," AIAA Paper No. 83-0034, 21st Aerospace Sciences Meeting, January 1983.

10. R. P. Reklis, and W. B. Sturek, "Surface Pressure Measurements on Slender Bodies at Angle of Attack at Supersonic Speeds," U.S. Army Ballistic Research Laboratory, Aberdeen Proving Ground, Maryland, ARBRL-MR-02876, November 1978. (AD A064097)

11. C. J. Nietubicz, and K. O. Opalka, "Supersonic Wind Tunnel Measurements of Static and Magnus Aerodynamic Coefficients for Projectile Shapes with Tangent and Secant Ogive Noses," U.S. Army Ballistic Research Laboratory, Aberdeen Proving Ground, Maryland, ARBRL-MR-02991, February 1980. (AD A083297)

12. D. S. Chaussee, J. L. Patterson, P. Kutler, T. Pulliam, and J. L. Steger, "A Numerical Simulation of Hypersonic Viscous Flows Over Arbitrary Geometries at High Angle of Attack," AIAA Paper 81-0050, January 1981.

13. F. Brandon, "private communication," U.S. Army Ballistic Research Laboratory, Aberdeen Proving Ground, Maryland.

14. A. B. Wardlaw, Jr., F. P. Baltakis, J. M. Solomon, and L. B. Hackerman "An Inviscid Computational Method for Tactical Missile Configurations," NSWC TR 81-457.

15. Unpublished range data, U.S. Army Ballistic Research Laboratory, Aberdeen Proving Ground, Maryland.

LIST OF SYMBOLS

a	=	speed of sound
C_A	=	axial force coefficient
$C_{A_{BL}}$	=	wall shear component of axial force coefficient
CP	=	normal force center of pressure
C_m	=	pitching moment coefficient
C_{m_α}	=	$dC_m/d\alpha$, slope of the pitching moment coefficent
$C_{M_{p\alpha}}$	=	$C_n/(PD/V)\alpha$, slope of the Magnus moment coefficient
C_n	=	Magnus (yawing) moment coefficient
C_N	=	normal force coefficient
C_{N_α}	=	$dC_N/d\alpha$, slope of the normal force coefficient
C_{p_w}	=	surface pressure component of Magnus force coefficient
C_Y	=	Magnus (side) force coefficient
C_{τ_x}	=	longitudinal wall shear component of Magnus force coefficient
C_{τ_ϕ}	=	circumferential wall shear component of Magnus force coefficient
D	=	diameter of model
e	=	total energy per unit volume of fluid, normalized by $\rho_\infty a_\infty^2$
$\hat{E}_s, \hat{F}, \hat{G}$	=	flux vectors of transformed gasdynamic equation
L	=	projectile length
M	=	Mach number
P	=	pressure normalized by $\rho_\infty a_\infty^2$
PD/V	=	non-dimensional spin rate about model axis
Re_D	=	Reynold's number based on diameter, $\rho_\infty M_\infty a_\infty D/\mu_\infty$

$\hat{Re}$ = Reynolds number, $\rho_\infty a_\infty D/\mu_\infty$

$\hat{S}$ = viscous flux vector

u,v,w = Cartesian velocity components along the x, y, z axis. respectively, normalized by a_∞

x,y,z = physical Cartesian coordinates

α = angle of attack

μ = coefficient of viscosity, normalized by free stream value,

ξ,η,ζ = computational coordinates in the axial, circumferential, and radial directions

ρ = density, normalized by free-stream density

ϕ = circumferential angular coordinate

Subscripts

∞ = free-stream conditions

wall = body surface values

DISTRIBUTION LIST

No. of Copies	Organization
12	Administrator Defense Technical Info Center ATTN: DTIC-DDA Cameron Station Alexandria, VA 22304-6145
1	HQDA DAMA-ART-M Washington, DC 20310
1	Commander US Army Materiel Command ATTN: AMCDRA-ST 5001 Eisenhower Avenue Alexandria, VA 22333-0001
8	Commander Armament R&D Center US Army AMCCOM ATTN: SMCAR-TDC SMCAR-TSS SMCAR-LCA-F Mr. D. Mertz Mr. E. Falkowski Mr. A. Loeb Mr. R. Kline Mr. S. Kahn Mr. H. Hudgins Dover, NJ 07801
1	Commander US Army Armament, Munitions and Chemical Command ATTN: SMCAR-ESP-L Rock Island, IL 61299
1	Director Benet Weapons Laboratory Armament R&D Center US Army AMCCOM ATTN: SMCAR-LCB-TL Watervliet, NY 12189
1	Commander US Army Aviation Research and Development Command ATTN: AMSAV-E 4300 Goodfellow Blvd St. Louis, MO 63120
1	Director US Army Air Mobility Research and Development Laboratory Ames Research Center Moffett Field, CA 94035
1	Commander US Army Communications - Electronics Command ATTN: AMSEL-ED Fort Monmouth, NJ 07703
1	Commander US Army Electronics Research and Development Command Technical Support Activity ATTN: DELSD-L Fort Monmouth, NJ 07703-5301
3	Commander US Army Missile Command ATTN: AMSMI-R AMSMI-RDK Dr. Bill Walker Mr. R. Deep Redstone Arsenal, AL 35898
1	Commander US Army Missile Command ATTN: AMSMI-YDL Redstone Arsenal, AL 35898
1	Commander US Army Tank Automotive Command ATTN: AMSTA-TSL Warren, MI 48090
1	Director US Army TRADOC Systems Analysis Activity ATTN: ATAA-SL White Sands Missile Range, NM 88002

DISTRIBUTION LIST

No. of Copies	Organization
1	Commander US Army Research Office P. O. Box 12211 Research Triangle Park, NC 27709-2211
1	Commander US Naval Air Systems Command ATTN: AIR-604 Washington, DC 20360
2	Commander David W. Taylor Naval Ship Research and Development Center ATTN: Dr. S. de los Santos Mr. Stanley Gottlieb Bethesda, Maryland 20084
2	Commander US Naval Surface Weapons Center ATTN: Dr. F. Moore Dahlgren, VA 22448
1	Commander US Naval Surface Weapons Center ATTN: Dr. U. Jettmar Silver Spring, MD 20910
1	Commander US Naval Weapons Center ATTN: Code 3431, Tech Lib China Lake, CA 93555
1	Commander US Army Development and Employment Agency ATTN: MODE-TED-SAB Fort Lewis, WA 98433
1	Director NASA Langley Research Center ATTN: NS-185, Tech Lib Langley Station Hampton, VA 23365

No. of Copies	Organization
1	Commandant US Army Infantry School ATTN: ATSH-CD-CSO-OR Fort Benning, GA 31905
1	AFWL/SUL Kirtland AFB, NM 87117
1	Air Force Armament Laboratory ATTN: AFATL/DLODL Eglin AFB, FL 32542-5000
3	Sandia Laboratories ATTN: Technical Staff, Dr. W.L. Oberkampf Aeroballistics Division 5631, H.R. Vaughn Dr. F. Blottner Albuquerque, NM 87184
1	Massachusetts Institute of Technology ATTN: Tech Library 77 Massachusetts Avenue Cambridge, MA 02139
1	Virginia Polytechnic Institute & State University ATTN: Dr. Clark H. Lewis Department of Aerospace & Ocean Engineering Blacksburg, VA 24061
1	University of Delaware Mechanical and Aerospace Engineering Department ATTN: Dr. J. E. Danberg Newark, DE 19711
3	Director NASA Ames Research Center ATTN: MS-227-8, L. Schiff MS-202A-14, D. Chaussee M. Rai Moffett Field, CA 94035

DISTRIBUTION LIST

Aberdeen Proving Ground

Dir, USAMSAA
ATTN: AMXSY-D
AMXSY-MP, H. Cohen

Cdr, USATECOM
ATTN: AMSTE-TO-F

Cdr, CRDC, AMCCOM,
ATTN: SMCCR-RSP-A
SMCCR-MU
SMCCR-SPS-IL

USER EVALUATION SHEET/CHANGE OF ADDRESS

This Laboratory undertakes a continuing effort to improve the quality of the reports it publishes. Your comments/answers to the items/questions below will aid us in our efforts.

1. BRL Report Number____________________ Date of Report__________

2. Date Report Received____________________

3. Does this report satisfy a need? (Comment on purpose, related project, or other area of interest for which the report will be used.)__________

4. How specifically, is the report being used? (Information source, design data, procedure, source of ideas, etc.)__________

5. Has the information in this report led to any quantitative savings as far as man-hours or dollars saved, operating costs avoided or efficiencies achieved, etc? If so, please elaborate.__________

6. *General Comments.* What do you think should be changed to improve future reports? (Indicate changes to organization, technical content, format, etc.)

CURRENT ADDRESS

Name

Organization

Address

City, State, Zip

7. If indicating a Change of Address or Address Correction, please provide the New or Correct Address in Block 6 above and the Old or Incorrect address below.

OLD ADDRESS

Name

Organization

Address

City, State, Zip

(Remove this sheet along the perforation, fold as indicated, staple or tape closed, and mail.)

FOLD HERE

Director
US Army Ballistic Research Laboratory
ATTN: AMXBR-OD-ST
Aberdeen Proving Ground, MD 21005-5066

NO POSTAGE NECESSARY IF MAILED IN THE UNITED STATES

OFFICIAL BUSINESS
PENALTY FOR PRIVATE USE, $300

BUSINESS REPLY MAIL
FIRST CLASS PERMIT NO 12062 WASHINGTON,DC

POSTAGE WILL BE PAID BY DEPARTMENT OF THE ARMY

Director
US Army Ballistic Research Laboratory
ATTN: AMXBR-OD-ST
Aberdeen Proving Ground, MD 21005-9989

FOLD HERE

END

FILMED

11-85

DTIC